Saleem H. Trier

Department of Medical Physics,
College of Science,
University of Al-Qadisiyah,
Al-Diwaniyah, IRAQ

Some Physical Properties of $Zn_{1-x}Gd_xO$ Composites Prepared by Solid Phase Reaction Method

Gd-doped ZnO samples prepared using the solid-phase reaction technique were investigated for their structural, optical, and dielectric properties. The presence of a hexagonal wurtzite phase was confirmed by XRD spectra, with the crystallite size distribution of 42.85, 45.38, and 47.13 nm. The grains showed an almost spherical shape, as revealed by FE-SEM images. The bonding behaviors of stretching modes such as O-H, O=C=O, and Zn-O were confirmed by FT-IR spectra. The optical energy gap gradually decreased (3.17, 3.18, and 3.20 eV, respectively), as confirmed by the optical absorption spectra. The PL spectra of all samples showed near-band emission, blue-shift emission, and green-shift emission peaks. The Gd-doped ZnO samples have a high dielectric, making them suitable as a coolant and insulator for transformers and charge storage devices. As the Gd concentration increases, the mobility and resistivity increase, according to Hall effect data.

***Keywords*:** Zinc oxide; Photoluminescence; Dielectrics; Solid phase reaction
Received: 23 September 2024; **Revised:** 02 January; **Accepted:** 09 January 2025

1. Introduction

Over the last few decades, bulk and nanostructured broadband semiconductors have garnered increasing attention from scientists and researchers. These materials have exceptional optical, electrical, magnetic, dielectric, and chemical characteristics [1]. Among these semiconductors, pure ZnO exhibits exceptional characteristics such as good optical transparency and a broad bandgap of 3.3 eV. In addition, the exciton binding energy of ZnO is 60 meV, much more than the thermal energy of 25 meV at room temperature. Moreover, cheap manufacturing cost, high thermal stability, non-toxicity, chemical stability, and mechanical stability of ZnO promote its usage in various applications. One of the most essential metal oxides is Zinc oxide (ZnO), which is used in many different applications such as chemical sensors [2], photocatalysts [3], dye-sensitized solar cells [4], spintronics, and others [5]. Doping ZnO with appropriate elements seems to improve its device fabrication properties. Numerous research groups have investigated transition metals such as Co, Mn, and Ni-doped ZnO [6]. Ferromagnetic properties are obtained by doping ZnO with rare earth metals [7].

Room-temperature ferromagnetic properties are demonstrated by Er-doped ZnO composites [8]. Ce-doped ZnO nanocrystal's luminescence properties show a decrease in emission intensity, consistent with the creation of additional surface defects [9]. ZnO:Nd^{3+} nanopowders were made at high temperatures using a regulated solid phase reaction technique [10]. Nd-doped ZnO has crisp visible emission, which holds great potential for applications that emit light. Gd, a beneficial dopant in rare earth metals, has drawn interest from researchers because of its fascinating uses in optoelectronic and magnetic devices. The addition of gadolinium (Gd) is of particular interest due to its f orbital effect when it is half full, which is believed to affect the photocatalytic activity of ZnO significantly. In this study, Gd is crucial in altering ZnO structural, optical, and dielectric properties when doped into the material.

The potential applications of Gd-doped ZnO are vast and inspiring. Energy harvesting devices can benefit from Gd doping in ZnO [11]. Spintronic applications can use sol-gel spin coating-produced Gd-doped ZnO thin films [12], whereas co-precipitation-produced (Gd, Co) co-doped ZnO nanotubes [13]. Through a solid-phase reaction, Gd^{3+}/Yb^{3+} co-doped ZnO phosphors were manufactured [14]. These applications, among others, demonstrate the wide-ranging potential of Gd-doped ZnO in various fields. Light-emitting diodes can be made with the synthetic phosphors. An effective photocatalyst may be made with the aid of r-GO-supported Gd-doped ZnO via the hydrothermal method [15]. Gd-doped ZnO thin films made using the co-sputtering technique demonstrated that Gd doping enhanced ZnO magnetic characteristics and caused the film to transition from diamagnetic to paramagnetic behavior [16]. Spray pyrolysis [17], the sol-gel method [18], magnetron sputtering [19], sonochemical methods [20], and other synthetic methods can be used to create ZnO nanostructures of different sizes and morphologies. Ma and Wang synthesized Gd-doped ZnO nanocrystals by vapor phase deposition using thermal evaporation [21]. Gd-doped ZnO nanorods were made by Obeid et al. using the thermal decomposition technique [22]. Several techniques have been used for sample synthesis. The sample prepared by solid phase reaction demonstrated a decreasing energy gap of ZnO as Gd concentration increased [23]. Gd-doped ZnO samples generated by the sonochemical technique exhibit superior

photocatalytic activity compared to pure ZnO, as revealed by Yayapao et al. [24].

Prepared by the wet chemical method, Gd-doped ZnO nanoparticles demonstrate that ZnO energy gap shrinks with increasing Gd doping concentration [25]. This observation is significant as it indicates that the energy gap of ZnO can be controlled and potentially reduced by increasing the Gd concentration, which could have implications for the material's optical and electrical properties. Gd:ZnO films with a hexagonal wurtzite structure were deposited using RF magnetron sputtering. Doping Gd causes a rise in defect concentration, which boosts deep-level emission [26]. Very high visible light luminescence performance is exhibited by pure and Gd-doped ZnO nanostructures generated via hydrothermal process exhibit highly high visible light luminescence performance, making them excellent materials for a variety of device applications such as sensors, LEDs, and so on [27]. Gd-doped ZnO nanoparticles were synthesized using the co-precipitation method, and Roy et al. examined their magnetic, structural, and optical responses [28].

The solid phase reaction method, used to manufacture Gd-doped ZnO powder samples at various concentrations (x= 0.0, 0.04, and 0.08), is cost-effective and environmentally friendly. It can produce non-uniform atomic mixtures without chemical agents, acids, or laborious chemical reactions. In fact, the solid phase reaction method is the least expensive among all the possible mixing techniques, and its use of non-hazardous chemicals ensures that it will not harm the environment. This reassures the practicality and sustainability of our research.

The x-ray diffraction (XRD), Fourier-transform infrared spectroscopy (FTIR), UV-visible spectroscopy, photoluminescence (PL) spectroscopy, impedance analyzer, and Hall effect measurements were utilized to ensure a comprehensive analysis. ZnO properties could be modified by doping it with rare earth elements. Gd doping among these rare earth metals has a noticeable impact on ZnO optical, dielectric, and magnetic characteristics. To the author’s knowledge, more research must be done on the ZnO-Gd dielectric characteristics. Therefore, this work presents a comprehensive analysis of the structural, optical, and dielectric properties of Gd-doped Zinc oxide, instilling confidence in the reliability of our findings, and aims to understand the effect of Gd in ZnO regarding its structural, optical, and dielectric properties. A series of ZnO powders doped with Gd at different values (0%, 4%, and 8%) were prepared. Different characterization techniques explored the composite powders' structural, optical, and dielectric properties. Gd in ZnO led to changes in the composite's morphological, optical, and dielectric properties, and this condition was exploited for its application in devices involving charge storage.

2. Experimental Part

The solid phase reaction, a method of significant importance in synthesizing complex oxides, involves chemical decomposition reactions. This method, which is relatively inexpensive and requires simple apparatus, is particularly noteworthy for its ability to produce complex oxides from simple oxides, carbonates, nitrates, and other metal salts. The procedure, which includes several annealing steps with multiple intermediate milling steps, is designed to increase the mixture's homogeneity and decrease the powder's particle size. The extra milling also makes the powder more active in the subsequent heat-treatment steps. Moreover, this method can prepare large volumes of powder relatively simply. The obtained powder shows relatively high agglomeration and, therefore, relatively large particle size, as well as relatively limited homogeneity. Pure ZnO and Gd-doped ZnO samples $Zn_{1-x}Gd_xO$ (x = 0.0, 0.04, and 0.08) were synthesized using a solid phase reaction. Using an electronic scale, the starting ingredients ZnO and Gd_2O_3 were weighed to guarantee accurate chemical readings. After thoroughly combining the ingredients, the particles were sintered for eight hours at 1000 °C at room temperature after being ground in a ball mill for long enough to prepare fine powders.

Before characterization, the mixture was dried and milled for one hour. Using XRD analysis, the structural characteristics of the prepared powder samples were examined in the 20-90° range. FTIR spectroscopy was used to identify the chemical functional groups in the synthesized samples. The surface morphology of the synthesized samples was examined using field-emission scanning electron microscopy (FE-SEM). In addition, energy-dispersive x-ray spectroscopy (EDX) was performed to determine the chemical composition of the samples. Atomic force microscopy (AFM) examined the samples' surface topography and surface roughness in contact mode. All prepared samples were optically examined using absorption spectra obtained using a UV-visible spectrophotometer, covering the wavelength range of 350-550nm. Tauc's plots were utilized to determine the optical energy gap of each prepared sample. The samples under investigation were also subjected to photoluminescence spectroscopy. An impedance analyzer was used to assess the powder samples after they were formed to determine the dielectric constant, and a hydraulic press was used to form pellets. A Hall effect measurement device was used to calculate mobility, resistivity, and mass concentration.

3. Results and Discussion

XRD was employed to investigate the creation of crystalline phases. The pure ZnO and Gd-doped ZnO samples $Zn_{1-x}Gd_xO$ (x= 0.0, 0.04, and 0.08) synthesized using the solid phase reaction method are shown in Fig. (1) with their XRD patterns. The XRD data were

obtained in the 2θ range of 20-90°. Sharp and intense peaks are visible in the XRD patterns, consistent with ZnO hexagonal wurtzite structure. The secondary phase of Gd_2O_3 is responsible for the extra peaks that emerged in the Gd-doped samples at 28.80° and 33.35°. The intensity of the diffraction peaks decreases with increasing Gd content. This decrease can be attributed to the reduced crystallite size or decreased crystallinity due to the ionic radius difference between dopant Gd^{3+} (0.93 Å) and host Zn^{2+} (0.74 Å) [29]. The Gd-doped samples show a shift to lower angles compared to pure ZnO. The lowered peak intensity and shift to lower angles confirm the appropriate incorporation of Gd into the ZnO host lattice. The Debye-Scherrer equation (1) was utilized to determine the crystallite size of the synthesized samples [30]

$$D = \frac{k\lambda}{\beta cos\theta} \quad (1)$$

In this equation, λ is the wavelength of the incident x-ray beam (1.540 Å), k is the shape factor (0.9), β represents the full-width at half maximum (FWHM) value in radians, whereas θ represents the Bragg diffraction angle

To determine the average crystallite size (D) of the produced powder samples, the preferred direction of the peak (101) was chosen as in Fig. (2).

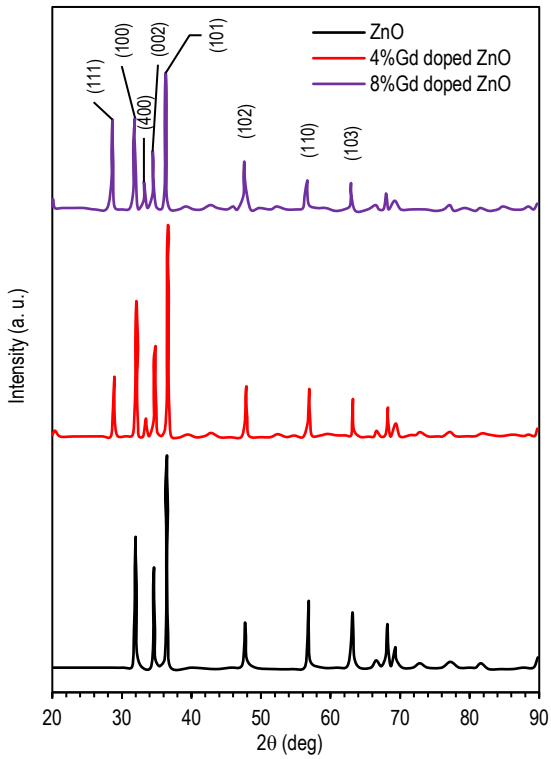

Fig. (1) XRD patterns of $Zn_{1-x}Gd_xO$ samples (x = 0.0, 0.04 and 0.08)

The results reveal that the average crystallite size (D) is within the range of 42.85, 45.38, and 47.13 nm, and the crystallite size of the doped ZnO samples is smaller than that of the pure ZnO samples as in table (1), which is also consistent with the earlier results [1,30,31]. A key factor influencing the prepared samples' crystallinity is Gd doping in the ZnO host lattice. This suggests that Gd doping influences grain growth and nucleation; increasing the concentration of Gd doping inhibits these processes by creating more cation vacancies, which causes the crystallite size to decrease and the peaks to shift to lower 2θ angles. These findings are corroborated by previous research [32, 33]. The Zn-O bond length is 1.95 Å since the ionic radius of Zn^{2+} is 0.74Å and the ionic radius of O^{2-} is 1.21Å. All samples had computed values that are marginally more than 1.95Å. Structural flaws, particularly oxygen vacancies, are revealed by this finding. Table (2) illustrates how Gd doping alters the Zn-O bond length, unit cell size, and lattice properties. Compared to unhoped ZnO, the crystallite parameter values of the doped samples are lower. This suggests that Gd^{3+} ions, which are replaced in the ZnO lattice, have a greater ionic radius than Zn^{2+} ions. Crystal flaws and an imbalance in the ZnO structure result from the filling of the Zn^{2+} ion lattice by Gd^{3+} ions.

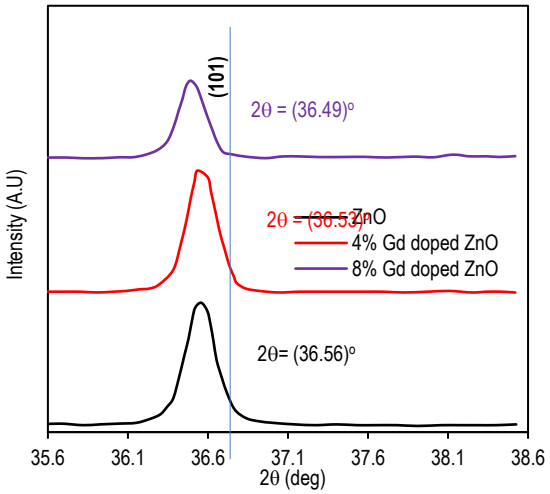

Fig. (2) XRD patterns of the (101) plane magnified

Table (1) Change of crystallite size, FWHM, and 2θ with Gd concentration for (101) preferred plane

Samples	2θ (deg)	Preferred direction	FWHM (deg)	Crystallite size (nm)
ZnO	36.56	(101)	0.0194	47.13
4%Gd:ZnO	36.53	(101)	0.0202	45.38
8%Gd:ZnO	36.49	(101)	0.0214	42.85

The unit cell volume of the hexagonal system is calculated as V = (0.866) a^2c. The lattice constant is the only factor that affects the unit cell volume. As shown in table (2), the unit cell volume decreases with increasing Gd concentration. This is because Gd^{3+} ideally replaces the Zn^{2+} in the lattice.

Figure (3) shows the surface morphology of undoped and Gd-doped ZnO samples analyzed using FE-SEM. Hexagonal grains were observed in each

sample, and the grains were homogeneously distributed throughout the sample. In contrast to the doped samples, the images of the doped samples show that the grains are denser and smaller in size. Doping causes an increase in the voids between the grains, which can be explained by the presence of substitution-related defects. When compared to the undoped sample, the images show that the grain size decreases with gadolinium doping and increases with increasing gadolinium doping percentage.

Table (2) Change of lattice constants and unit cell volume with Gd concentration

Samples	a(nm)	c(nm)	c/a	Cell volume $(nm)^3$
ZnO	3.253	5.211	1.6019	47.75
4%Gd:ZnO	3.250	5.207	1.6021	47.63
8%Gd:ZnO	3.248	5.202	1.6017	47.53

The EDX and FE-SEM results of pure and Gd-doped ZnO samples are displayed in Fig. (3). The granules have a roughly spherical form, as seen in FE-SEM micrographs [1]. Good grain aggregation is the outcome of the grains being retained together. The primary cause of the aggregation is the creation of bonds between adjacent particles. EDX verified the components of the powder sample. The Gd-doped ZnO sample's spectrum reveals the presence of Zn, O, and Gd, whereas the pure ZnO sample's spectrum only reveals the presence of oxygen and zinc ions. The Gd^{3+} has successfully replaced the dopant in the ZnO, as shown by the EDX data [34].

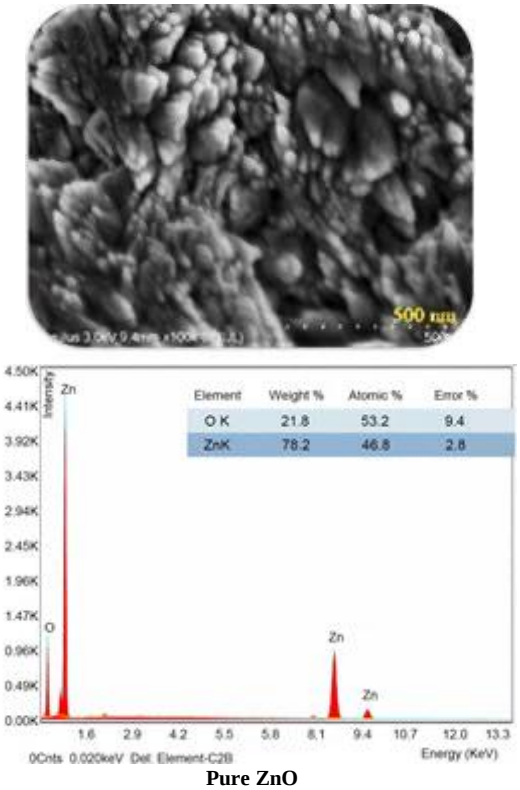

Pure ZnO

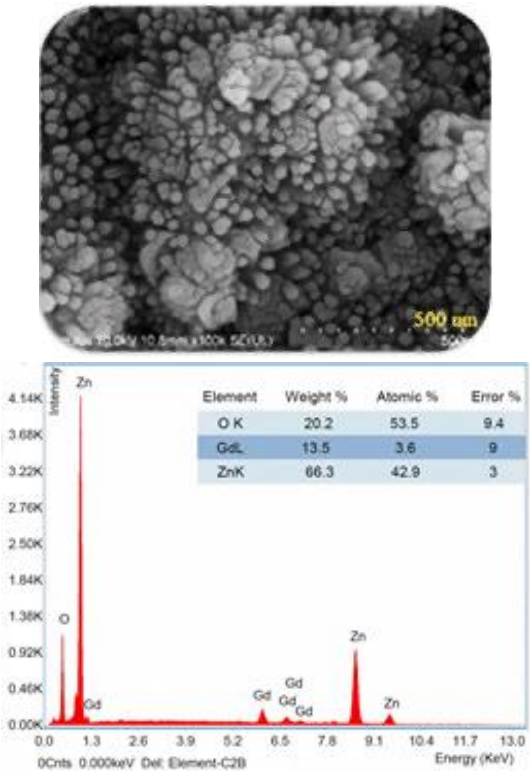

4% Gd-doped ZnO

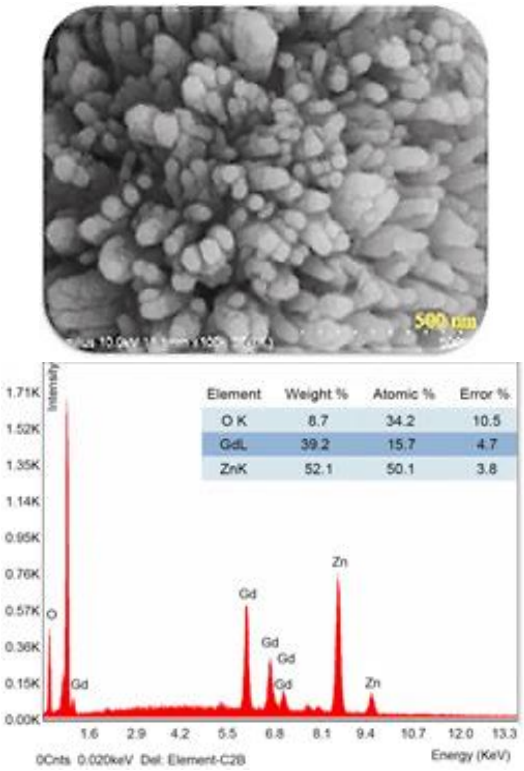

8% Gd-doped ZnO

Fig. (3) FE-SEM images with EDX spectra of $Zn_{1-x}Gd_xO$ (x = 0.0, 0.04, and 0.08) samples

Nanoflower structures can be observed in the surface morphology by doping Gd on ZnO films. The nanoflower structure becomes denser and increases in

crystallite size, especially in Gd-doped ZnO (8 %) films.

Figure (4) displays the FTIR spectra of samples of $Zn_{1-x}Gd_xO$ (x = 0.0, 0.04, and 0.08). The functional groups in $Zn_{1-x}Gd_xO$ samples were determined by FTIR measurements in the 500-4000 cm^{-1} range. ZnO distinctive absorption band is visible at low wavenumbers [35]. It can be seen in the investigated samples at around 529 cm^{-1}, which aligns with the ZnO bond stretching vibration mode. Because Gd^{3+} dopants replace Zn^{2+} ions in the Gd-doped ZnO lattice, the strength of the Zn-O stretching peak is reduced in Gd-doped ZnO samples [36].

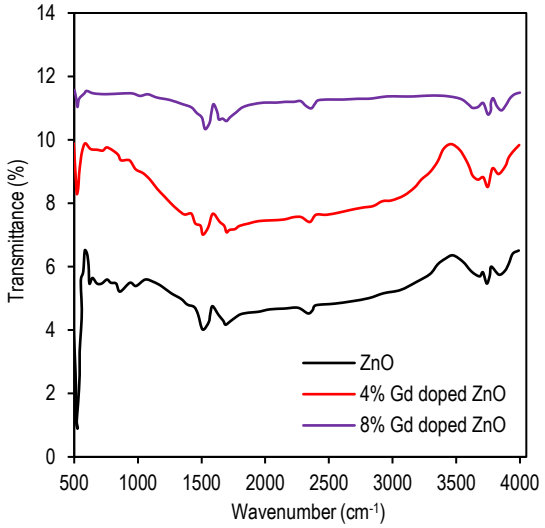

Fig. (4) FTIR spectra of $Zn_{1-x}Gd_xO$ (x = 0, 0.04, and 0.08) samples

The peak at 2353 cm^{-1} is caused by the adsorption of O=C=O on the surface during the FTIR procedure [2,30,37]. Some water molecules probably arrived in the air because the samples were processed in an ambient atmosphere. The absorption band at 3673-3845 cm^{-1} represents the O-H stretching vibration, which is nearly in line with the findings of previous studies [30,38]. Water molecules that have been adsorbed on the ZnO surface cause the absorption band to form at 1522-1695 cm^{-1} [38].

Figure (5) shows the absorption spectra of the prepared samples $Zn_{1-x}Gd_xO$ (x=0.0, 0.04, and 0.08) in the wavelength range of 350-550 nm. Numerous variables influence these samples' absorbance, including surface roughness, oxygen deficit, and particle size. The figure illustrates that the absorption edge changes to a higher wavelength direction when Gd is added to ZnO samples.

The Tauc's plot was used to calculate the optical energy gap values of all synthesized samples, and the optical energy gaps of the pure ZnO and Gd-doped ZnO samples were found to be 3.2, 3.18, and 3.17 eV, respectively as in Fig. (6). The energy gap values of the doped samples are lower than the pure sample; these results were compared with previous research [1,18,39]. Doping with Gd generates new electronic energy levels or subbands in the ZnO energy gap. New subbands merge or electronic energy levels with the band of conduction. To produce a continuous energy band, reducing the energy gap even further [18,40].

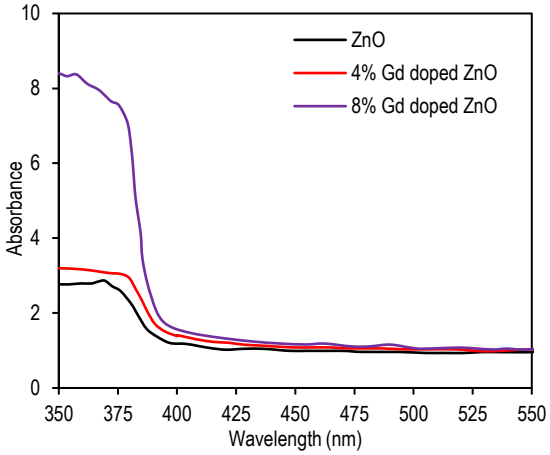

Fig. (5) The absorption spectra of $Zn_{1-x}Gd_xO$ (x = 0.0, 0.04, and 0.08) samples

The photoluminescence (PL) spectra of room-temperature powder samples of pure ZnO and Gd-doped ZnO are displayed in Fig. (7). At a wavelength of 390nm, photoluminescence examination was carried out on powder samples of pure ZnO and ZnO doped with Gd. The processed samples feature three emission bands, as seen in Fig. (8). The first represents a violet emission peak centered at 420nm, the second represents a blue emission peak centered at 457nm, and the third represents a green emission peak centered at 497nm. The violet emission around 420nm occurs due to transitions between the conduction band and acceptor levels associated with zinc vacancies [32,41].

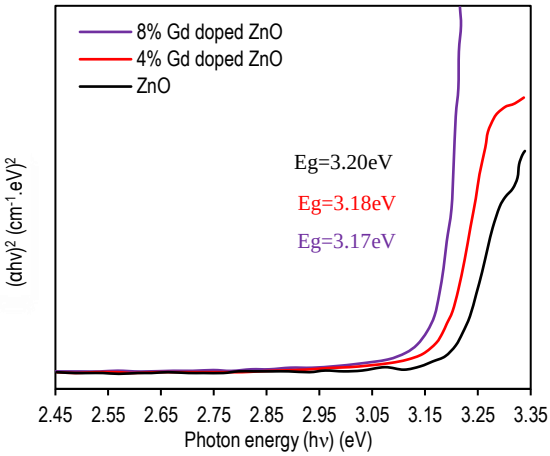

Fig. (6) Optical energy gap of $Zn_{1-x}Gd_xO$ (x = 0.0, 0.04, and 0.08) samples

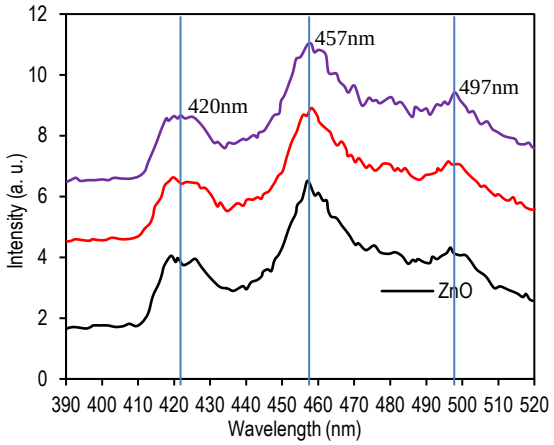

Fig. (7) PL spectra of $Zn_{1-x}Gd_xO$ (x = 0.0, 0.04 and 0.08) samples

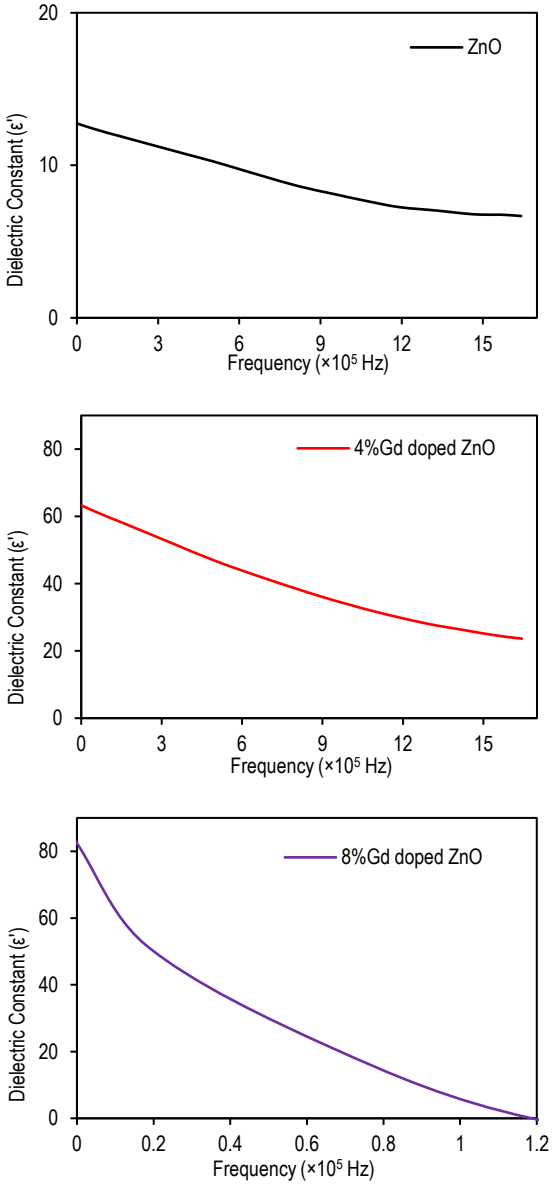

Fig. (8) Dielectric constant of $Zn_{1-x}Gd_xO$ (x = 0.0, 0.04 and 0.08) samples

Blue fluorescence appears at 457 nm in all samples due to electronic transitions between vacancy (VZn) levels and zinc interstitial (Zni) [32,42,43]. Green emission is seen at 497 nm in all samples, ascribed to electronic transitions brought on by energy gap defect levels. Potential flaws could exist in the zinc or oxygen interspaces [44]. According to the PL results, the samples have many microstructural flaws, which indeed aid in doping the ZnO samples to adjust their electrical characteristics.

Figure (8) shows a plot of the dielectric variation with frequency at room temperature. The dielectric behavior of nanostructured materials is influenced by several phenomena, including electronic, ionic, dipole, and space charge polarization. The dielectric constant values of the manufactured samples were obtained using the following equation:

$$\varepsilon' = Cd/\varepsilon_o A \quad (2)$$

where C represents the sample's capacitance and ε_o its free space dielectric constant, respectively, and the thickness and area of the grain are denoted by d and A

The dielectric constant (ε') decreases with increasing applied electric field frequency in pure and Gd-doped ZnO samples. The Maxwell-Wagner model, which postulates that poorly conducting grain boundaries separate well-conducting grains in dielectric structures, can explain this result; this has been explained in earlier studies [45].

Because of the high resistance at grain boundaries, electrons can accumulate and cause polarization by hopping. Furthermore, at low frequencies, persistent dipoles can align themselves along the direction of the electric field and externally applied, increasing the dielectric characteristics. The electrons' jumping frequency cannot keep up with the increasing frequency of the external electric field. As a result, there is less polarization since the electrons cannot cross the grain boundaries. The above explanation and the study's findings align with Koops' phenomenological theory [46]. Numerous studies have found that Gd-doped ZnO lattice decreases dielectric constant.

Franco Jr. et al. [40] reported a similar outcome, except in this investigation, Gd-doped ZnO increased the dielectric constant. Different ratios of Gd to ZnO result in higher concentrations of charge carriers and oxygen vacancies. As a result, the effects that generate dipole moment interact more. Due to surface polarization in the sample, the polarization drastically lowers and the dielectric constant rapidly drops when the Gd content in the ZnO lattice rises to 8%. The existence of several interfacial polarizations in the material could be a plausible explanation for this outcome [32].

The bulk concentration, Hall mobility, resistivity, and conductivity changes for varying Gd concentrations are displayed in figures (9) and (10). The bulk concentration falls with Gd doping while the

resistivity and mobility increase. The drop in bulk concentration can be explained by an increase in grain boundary defects, which serve as free carrier traps. Charge carrier dispersion is the primary determinant of Hall mobility and resistivity. The most frequent scattering centers are the grain boundaries, phonons, crystal defects, and ionized impurities. Therefore, higher Hall mobility and resistivity may result from the impact of ionized impurities on the scattering process. Other rare earth metals, such as Er and Yb-doped ZnO, have shown comparable outcomes [47].

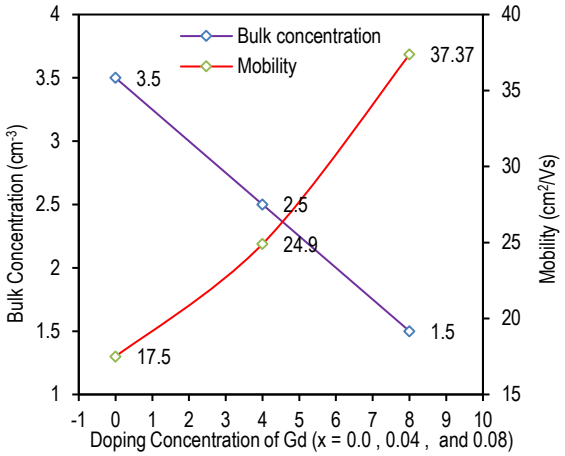

Fig. (9) Changes in Gd concentrations and their effects on bulk concentration and mobility

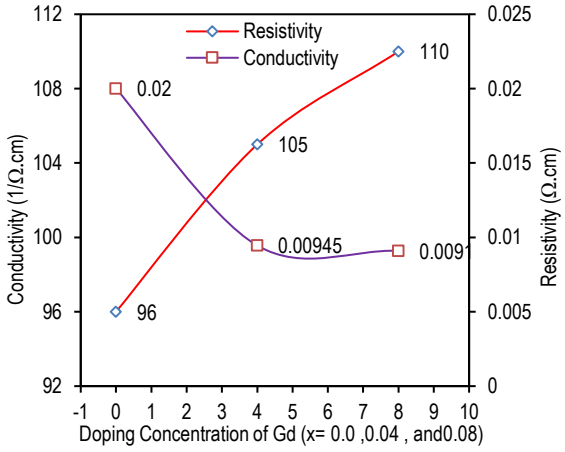

Fig. (10) Change in resistivity and conductivity about various Gd concentrations

4. Conclusions

Using the solid phase reaction method, Gd-doped ZnO ($Zn_{1-x}Gd_xO$) samples were prepared, and the structure of a hexagonal wurtzite was validated. The enhanced optical and dielectric characteristics of the Gd-doped ZnO are primarily due to their increased active surface area. The prepared grains roughly showed spherical morphology and ability to form a well-agglomerated structure. PL measurements reveal peaks at the near-band, blue emission, and green emission in pure and Gd-doped ZnO samples. The Gd-doped ZnO powder samples had great dielectric values, suggesting they would be a good option for charge storage applications. The Gd-doped ZnO sample has a high dielectric constant, making it suitable as a coolant and insulator in transformers and charge storage devices. Because of its large active surface area, the composite can be made into high-performance solar cells and gas sensors.

References

[1] K. Punia et al., "A Comprehensive Study on the Impact of Gd Substitution on Structural, Optical and Magnetic Properties of ZnO Nanocrystals", *J. Alloys Comp.*, 868 (2021) 159142.

[2] K.S. Weißenrieder and J. Müller, "Conductivity Model for Sputtered ZnO-Thin Film Gas Sensors", *Thin Solid Films*, 300 (1997) 30-41.

[3] S. Selvaraj et al., "Synthesis and Photocatalytic Activity of Gd Doped ZnO Nanoparticles for Enhanced Degradation of Methylene Blue under Visible Light", *Mater. Sci. Semicond. Process.*, 103 (2019) 104622.

[4] A. Umar et al., "Direct Growth of ZnO Nanosheets on FTO Substrate for Dye-Sensitized Solar Cells Applications", *J. Nanosci. Nanotech.*, 10 (2010) 6666-6671.

[5] C. Ronning et al., "Manganese-Doped ZnO Nanobelts for Spintronics", *Appl. Phys. Lett.*, 84 (2004) 783-785.

[6] R.K. Singhal et al., "Effect of Co and O Defects on Ferromagnetism in Co-Doped ZnO: An X-Ray Absorption Spectroscopic Investigation", *Physica B: Cond. Matter*, 530 (2018) 1-6.

[7] A.A. Dakhel and M. El-Hilo, "Ferromagnetic Nanocrystalline Gd-Doped ZnO Powder Synthesized by Coprecipitation", *J. Appl. Phys.*, 107 (2010) 123905.

[8] R. John and R. Rajakumari, "Synthesis and Characterization of Rare Earth Ion Doped Nano ZnO", *Nano-Micro Lett.*, 4 (2012) 65-72.

[9] A. George et al., "Detailed of X-Ray Diffraction and Photoluminescence Studies of Ce Doped ZnO Nanocrystals", *J. Alloys Comp.*, 509 (2011) 5942-5946.

[10] K. Jayanthi et al., "Observation of Nd3+ Visible Line Emission in ZnO:Nd^{3+} Prepared by a Controlled Reaction in the Solid State", *J. Phys. D: Appl. Phys.*, 46 (2013) 325101.

[11] S. Goel et al., "Ferroelectric Gd-Doped ZnO Nanostructures: Enhanced Dielectric, Ferroelectric and Piezoelectric Properties", *Mater. Chem. Phys.*, 202 (2017) 56-64.

[12] N.C. Ani et al., "Investigation of Spin Polarization in Gd-Doped ZnO Films for High-Performance Organic Spintronic Devices", *Mater. Sci. Eng. B*, 276 (2022) 115536.

[13] R. Khan et al., "Room Temperature Dilute Magnetic Semiconductor Response in (Gd, Co) Co-Doped ZnO for Efficient Spintronics Applications", *RSC Adv.*, 12 (2022) 36126-36137.

[14] M. Chakraborty et al., "Photoluminescence and EPR Investigation in ZnO:Gd^{3+}, Yb^{3+} Phosphors for Application in Light Emitting Diode", *Mater. Sci. Semicond. Process.*, 166 (2023) 107758.

[15] B. Palanivel et al., "Effect of RGO Support on Gd@ZnO for UV-Visible-Light Driven Photocatalytic Organic

Pollutant Degradation", *J. Rare Earths*, 41 (2023) 1525-1531.
[16] N.A. Raship et al., "Enhanced Magnetic Properties of Gd-Doped ZnO by Varying the Gd Concentration via Co-Sputtering Technique", *Mater. Sci. Forum*, 1114 (2024) 15-20.
[17] H. Chen et al., "Optical Properties of Ti-Doped ZnO Films Synthesized via Magnetron Sputtering", *J. Alloys Comp.*, 534 (2012) 59-63.
[18] N. Aggarwal et al., "Structural, Optical and Magnetic Properties of Gadolinium-Doped ZnO Nanoparticles", *J. Mater. Sci. Mater. Electron.*, 27 (2016) 13006-13011.
[19] M. Rouchdi et al., "Synthesis and Characteristics of Mg Doped ZnO Thin Films: Experimental and *Ab-Initio* Study", *Results Phys.*, 7 (2017) 620-627.
[20] A. Phuruangrat et al., "Synthesis and Characterization of Europium-Doped Zinc Oxide Photocatalyst", *J. Nanomater.*, 2014 (2014) 367529.
[21] X. Ma and Z. Wang, "The Optical Properties of Rare Earth Gd Doped ZnO Nanocrystals", *Mater. Sci. Semicond. Process.*, 15 (2012) 227-231.
[22] M.M. Obeid et al., "Unraveling the Effect of Gd Doping on the Structural, Optical, and Magnetic Properties of ZnO Based Diluted Magnetic Semiconductor Nanorods", *RSC Adv.*, 9 (2019) 33207-33221.
[23] M.K. Gora et al., "Electronic, Structural and Optical Properties of Gd-Doped ZnO Powder Synthesized by Solid-State Reaction Method", *Bangladesh J. Sci. Ind. Res.*, 58 (2023) 53-64.
[24] O. Yayapao et al., "Synthesis and Characterization of Highly Efficient Gd Doped ZnO Photocatalyst Irradiated with Ultraviolet and Visible Radiations", *Mater. Sci. Semicond. Process.*, 39 (2015) 786-792.
[25] D. Sahu et al., "Effect of Gd Doping on Structure and Photoluminescence Properties of ZnO Nanocrystals", *Mater. Res. Exp.*, 4 (2017) 114001.
[26] X.Y. Yi et al., "Structural, Morphological, Photoluminescence and Photocatalytic Properties of Gd-Doped ZnO Films", *Thin Solid Films*, 636 (2017) 339-345.
[27] K.A. Malik et al., "Trap Assisted Visible Light Luminescent Properties of Hydrothermally Grown Gd Doped ZnO Nanostructures", *Vacuum*, 183 (2021) 109832.
[28] S. Roy et al., "Effects of Gd Ions Doping on the Microstructural, Magnetic and Optical Properties in ZnO Nanocrystals", *Bull. Mater. Sci.*, 45 (2022) 193.
[29] S. Sambasivam et al., "Intense Violet-Blue Emission and Paramagnetism of Nanocrystalline Gd^{3+} Doped ZnO Ceramics", *J. Adv. Ceram.*, 4 (2015) 300-306.
[30] L. Pawlowski, "The Science and Engineering of Thermal Spray Coatings", 2nd ed., John Wiley & Sons (2007), p. 306.
[31] H. Khajuria et al., "Surfactant Assisted Sonochemical Synthesis and Characterization of Gadolinium Doped Zinc Oxide Nanoparticles", *Acta Chimica Slovenica*, 62 (2015) 849-858.
[32] S. Das et al., "Effect of Gd Doping Concentration and Sintering Temperature on Structural, Optical, Dielectric and Magnetic Properties of Hydrothermally Synthesized ZnO Nanostructure" *J. Alloys Comp.*, 708 (2017) 231-246.
[33] S.H. Trier, "Study of Optical, Electrical, and Structural Properties of Zinc-Doped CdTe Films by Chemical Bath Deposition", *Iraqi J. Appl. Phys.*, 20 (2024) 363-368.
[34] P.U. Aparna et al., "Structural and Dielectric Studies of Gd Doped ZnO Nanocrystals at Room Temperature", *J. Mater. Sci. Chem. Eng.*, 4 (2016) 79-88.
[35] A.A. Ibrahim et al., "Synthesis and Characterization of Gd-Doped ZnO Nanopencils for Acetone Sensing Application", *Sci. Adv. Mater.*, 7 (2015) 1241-1246.
[36] A. Khataee et al., "Sonocatalytic Degradation of a Textile Dye Over Gd-Doped ZnO Nanoparticles Synthesized through Sonochemical Process", *Ultrason. Sonochem.*, 23 (2015) 219-230.
[37] U.P. Gawai et al., "Influence of Gd Substitutionon Different Properties of ZnO Nanoparticles", *IOSR J. Eng.*, 9 (2019) 51-57.
[38] O. Oprea et al., "Photoluminescence, Magnetic Properties and Photocatalytic Activity of Gd^{3+} Doped ZnO Nanoparticles", *Digest J. Nanomater. Biostruct.*, 7 (2012) 1757-1766.
[39] P. Bharathi et al., "Growth and Influence of Gd Doping on ZnO Nanostructures for Enhanced Optical, Structural Properties and Gas Sensing Applications", *Appl. Surf. Sci.*, 499 (2020) 143857.
[40] A. Franco Jr. and H.V.S. Pessoni, "Effect of Gd Doping on the Structural, Optical Band-Gap, Dielectric and Magnetic Properties of ZnO Nanoparticles", *Physica B*: *Cond. Matter*, 506 (2017) 145-151.
[41] P.S. Venkatesh et al., "Role of Point Defects on the Enhancement of Room Temperature Ferromagnetism in ZnO Nanorods", *Cryst. Eng. Comm.*, 14 (2012) 4713-4718.
[42] X. Wei et al., "Blue Luminescent Center and Ultraviolet-Emission Dependence of ZnO Films Prepared by Pulsed Laser Deposition", *Japanese J. Appl. Phys.*, 45 (2006) 8586.
[43] H. Zeng et al., "Blue Luminescence of ZnO Nanoparticles Based on Non-Equilibrium Processes: Defect Origins and Emission Controls", *Adv. Func. Mater.*, 20 (2010) 561-572.
[44] Y. Gong et al., "Origin of Defect-Related Green Emission from ZnO Nanoparticles: Effect of Surface Modification", *Nanoscale Res. Lett.*, 2 (2007) 297.
[45] V. Raghavan, **"Material Science and Engineering"**, 5th ed., New Delhi (2010) p. 414.
[46] C.G. Koops, "On the Dispersion of Resistivity and Dielectric Constant of Some Semiconductors at Audio Frequencies", *Phys. Rev.*, 83 (1951) 121-124.
[47] S.D. Senol, "Hydrothermal Derived Nanostructure Rare Earth (Er, Yb)-Doped ZnO: Structural, Optical and Electrical Properties", *J. Mater. Sci. Mater. Electron.*, 27 (2016) 7767-7775.

